

Separating Xylene Isomers by Commensurate Stacking of *p*-Xylene within Channels of MAF-X8**

Ariana Torres-Knoop, Rajamani Krishna, and David Dubbeldam*

Abstract: The development of energy-efficient processes for selective separation of *p*-xylene from mixtures with its isomers is of vital importance in the petrochemical industries. Current industrial practice uses BaX zeolite that has high adsorption selectivity for *p*-xylene. Finding *para*-selective structures is challenging. With state-of-the-art simulation methodologies we systematically screened a wide variety of zeolites and metal–organic frameworks (MOFs). Our investigations highlight the crucial importance of the channel dimension on the separation. MAF-X8 is particularly noteworthy because the channel dimensions and geometry allow “commensurate stacking” which we exploit as a separation mechanism at saturation conditions. Due to a significantly improved capacity compared to BaX, the cycle times for *p*-xylene with MAF-X8 are found to be about a factor of 4.5 longer. This is expected to result in significant process improvements.

The separation of C₈ aromatic hydrocarbons is of great importance in the petrochemical industries. Some mixed xylenes are used for blending in gasoline, as solvents, and in the printing, rubber, and leather industries.^[1] Most mixed xylenes are separated and the individual isomers consumed in specific end-uses. *para*-Xylene, the most valuable of the isomers, is primarily used as a feedstock with purity requirements of 99% + for terephthalic acid or dimethyl terephthalate production, whose end-use includes polyester fibers and polyethylene terephthalate (PET) resins for beverage bottles.^[2] The separation of C₈ aromatic hydrocarbons is difficult because of the small differences in the boiling points (Figure 1). There are, however, significant differences in the freezing points that allow fractional crystallization to be used for separations.^[3] The differences in the freezing points arise because of differences in the stacking efficiency of molecules. *para*-Xylene has the highest freezing point because the molecules stack most efficiently; pure *p*-xylene crystals are the first to emerge from the solution. However, the energy requirements for fractional crystallization are high because of

the need to cool to temperatures of about 220 K. Selective adsorption of xylene isomers within the pores of ordered crystalline microporous materials is an energy efficient alternative to fractional crystallization.^[4] In industrial processing, the feed to the xylene separation unit is most commonly in the liquid phase, and the operation is performed under conditions of pore saturation. At these conditions, differences in saturation capacity are of great importance in determining separations (as explained in detail in Section S5). Because of the low *p*-xylene content of the feed it is often easier to reach a high productivity with *p*-xylene-selective adsorbents.^[4]

Thanks to early simulation work on xylenes in zeolites, for example by Snurr et al.,^[5] molecular simulations have now sufficiently evolved in speed and accuracy that large-scale screening studies have become feasible. Moghadam and Düren^[6] found that small-pore structures are *para*-selective and slightly larger pores are *ortho*-selective. However, this *para*-selectivity mechanism is based on “sieving”: the channel-dimensions are selected such that *p*-xylene is adsorbed and the larger *o*- and *m*-xylene are excluded from the channels. Sieving is therefore usually associated with small-pore systems with low *p*-xylene loadings. Moreover, such sieving is unable to separate *p*-xylene from ethylbenzene because of the diffusional limitations in such systems.


To search for systems that are superior to the current technology (BaX zeolite adsorbent used in UOP Parex and IFP Eluxyl, which employ simulated moving beds^[4,7,8]), we require 1) a high *para*-selective structure, 2) with a high pore volume, and 3) a structure that is able to operate near or at saturation conditions. In this work, we show that these goals can be achieved by exploiting “commensurate stacking”.

Commensurate stacking is much like stacking books on a bookshelf. Figure 1 shows a prototypical stacking of *o*- and *p*-xylene in a carefully chosen rectangular channel system. A MOF with channels of 0.85 nm allows the most efficient stacking of *o*-xylene. Channels of 1 nm are desirable for stacking *p*-xylene. In a 1 nm system, *p*-xylene is able to make full use of all the available pore volume and has a strong interaction, adsorbing flat on a wall while both methyl-groups interact with a sidewall. For molecules with different dimensions four effects occur: 1) “wider” molecules (like *o*- and *m*-xylene) will be able to stack less molecules per channel-length, 2) “longer” molecules (ethylbenzene) have to align obliquely and therefore also stack less molecules per channel-length, 3) “shorter” molecules (*o*- and *m*-xylene) will have a less optimal interaction with the pore structure; 4) more bulky molecules (ethylbenzene) are unable to form commensurate layers and will therefore have a lower saturation loading. The strategy we adopt in this work is to exploit

[*] A. Torres-Knoop,^[+] Prof. Dr. R. Krishna,^[+] Dr. D. Dubbeldam^[+]
Van't Hoff Institute for Molecular Sciences
University of Amsterdam
Science Park 904, 1098 XH Amsterdam (The Netherlands)
E-mail: D.Dubbeldam@uva.nl
Homepage: <http://molimol.sim.chem.uva.nl>

[+] These authors contributed equally to this work.

[**] This work is supported by the Netherlands Research Council for Chemical Sciences (NWO/CW) through a VIDI grant (D.D.).

 Supporting information for this article (adsorption and breakthrough simulation results) is available on the WWW under <http://dx.doi.org/10.1002/anie.201402894>. Figure numbers starting with S refer to Figures in the Supporting Information.

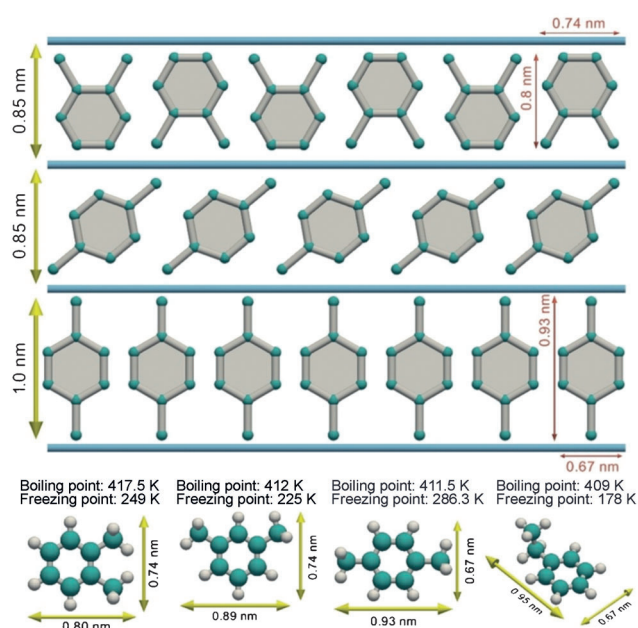


Figure 1. Schematic representation of “commensurate stacking” of xylenes in rectangular channels. The yellow arrows denote the characteristic lengths of the molecules, which have to be commensurate with the channel dimensions. Channels of about 0.85 nm in size allow an efficient stacking of *o*-xylene molecules. The same channel size forces *p*-xylene molecule to align obliquely, reducing the adsorption of *p*-xylene compared to *o*-xylene. A *p*-xylene stacking would require channel dimensions of about 1.0 nm.

differences in the stacking efficiencies of C₈ aromatic hydrocarbons within the MOF channels.

Ortho-selective structures: The adsorption of ethylbenzene as well as *o*-, *m*-, and *p*-xylenes within the one-dimensional, lozenge-shaped rhombohedral channels of MIL-47(V) of approximately 0.85 nm was considered. Adsorption within the channels of MIL-47(V) favors *o*-xylene because the molecules can most effectively stack along the channel length.^[9,10] Essentially, MIL-47(V) offers the appropriate “bookshelf” structure that is required to optimally stack *o*-xylene molecules^[8] (see Figure 2). Note that the channel dimensions of MIL-47(V) (and also of MIL-53, to be discussed next) is not large enough to allow *p*-xylene to stack vertically; these molecules align obliquely along the channel length (Figures S9a and S13a, respectively).

Breakthrough simulations for four-component *o*-xylene/*m*-xylene/*p*-xylene/ethylbenzene (Figure S11a) show the

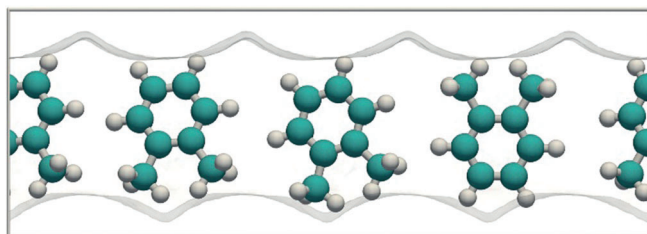


Figure 2. Snapshot of *o*-xylene in MIL-47 at 433 K. MIL-47 offers a 0.85 nm “bookshelf” which optimally stacks molecules that are commensurate with this dimension (i.e. *o*-xylene).

sequence of breakthroughs in a fixed-bed adsorber as ethylbenzene, *p*-xylene, *m*-xylene, and *o*-xylene. This is in agreement with the experimental breakthroughs reported by Finsy et al.^[11] The computed six-component breakthroughs of *o*-xylene/*m*-xylene/*p*-xylene/ethylbenzene/benzene/toluene in MIL-47 (Figure S11b) show that the presence of benzene and toluene in the fluid mixture does not alter the sequence of breakthroughs.

The framework structure of MIL-53(AI) is similar to that of MIL-47(V). The sequence of breakthroughs (Figure S15) is in qualitative agreement with experiments of Remy et al.^[12] Their work indicates that guest-induced structural changes of MIL-53(AI) also have to be considered in quantitative modeling of the breakthrough characteristics.

Fang et al.^[13] report pulse-breakthrough simulations for four-component *o*-xylene/*m*-xylene/*p*-xylene/ethylbenzene in MOF-CJ3 that clearly indicate adsorption selectivity toward *o*-xylene. MOF-CJ3 has square channels of approximately 0.8 nm size. The rationalization of *o*-xylene-selective adsorption is expected to be similar to that of MIL-47. CBMC simulations of pure component isotherms confirm that the adsorption is selective to the *ortho* isomer. Breakthrough simulations for four-component *o*-xylene/*m*-xylene/*p*-xylene/ethylbenzene in MOF-CJ3 show the hierarchy of breakthroughs to be ethylbenzene, *p*-xylene, *m*-xylene, and *o*-xylene (Figure S19). This hierarchy is not influenced by the presence of benzene and toluene in the feed mixture. For comparison with the pulse chromatographic experiments of Fang et al.,^[13] we also conducted pulse-breakthrough simulations. The pulse-chromatographic simulations (Figure S3) indicate that ethylbenzene and *p*-xylene peak at nearly the same time, in precise agreement with the experiments. The subsequent breakthroughs of *m*-xylene and *o*-xylene are in good agreement with the experimental data, albeit on a different time scale.

Nicolau et al.^[14] report experimental breakthrough data for C₈ hydrocarbons in beds packed with Zn(bdc)dabco, a framework that has two types of intersecting channels of about 0.75 nm × 0.75 nm along the x-axis. The sequence of breakthroughs of xylene isomers is *p*-xylene, *m*-xylene, and *o*-xylene.

Bárcia et al.^[15] and Moreira et al.^[16] report breakthrough data for C₈ aromatic hydrocarbons in UiO-66(Zr), a zirconium-based metal-organic framework (MOF). Its cubic rigid 3D pore structure consists of an array of octahedral cavities with 1.1 nm diameter, and tetrahedral cavities with 0.8 nm diameter. The two types of cages are connected through narrow triangular windows of approximately 0.6 nm. The sequence of experimental breakthroughs of xylene isomers is *p*-xylene, *m*-xylene, and *o*-xylene. The adsorption selectivity is in favor of *o*-xylene; this is most likely due to the more compact configuration of *o*-xylene that allows preferential location in the smaller tetrahedral cages of UiO-66. The separation performance is strongly influenced by intracrystalline diffusion considerations because of the small windows at the entrance to the cages.

All the MOFs (MIL-47(V), MIL-53(AI), MOF-CJ3, UiO-66, and Zn(bdc)dabco) discussed in the foregoing paragraph are selective for the adsorption of *o*-xylene, and less suitable

for use in industrial practice. Let us turn our attention to MOFs that have the desired selectivity towards *p*-xylene.

Para-selective structures: MIL-125(Ti) comprises of two different types of cages: larger 1.2 nm octahedral cages, and smaller tetrahedral 0.6 nm cages. Those are connected through narrow triangular windows of 0.5 nm. Amino functionalization of the benzene linker yields MIL-125(Ti)-NH₂. Due to the protrusion of the amino groups in the pore space the pore space of MIL-125(Ti)-NH₂ is slightly smaller than that in MIL-125(Ti).

The CBMC pure component isotherm for both MIL-125(Ti) and MIL-125(Ti)-NH₂, together with breakthrough simulations (Figure S23 and S27, respectively), show that these materials have selectivity towards the *para* isomer. The experimental data of Vermoortele et al.^[17] and Moreira et al.^[18,19] on breakthroughs of xylene isomers in MIL-125(Ti) and MIL-125(Ti)-NH₂, appear to confirm that these materials have the desirable selectivity towards *p*-xylene. However, the breakthrough experiments also show that the selectivity towards *p*-xylene appears to depend on the concentration of ethylbenzene in the feed stream. Indeed, for a range of feed compositions, *p*-xylene and ethylbenzene breakthrough at the same time. This indicates that both MIL-125(Ti) and MIL-124(Ti)-NH₂ are unlikely to be considered as suitable adsorbents because industrial feed mixtures invariably contain a sizable proportion of ethylbenzene.

CBMC simulation data for the adsorption of C₈ hydrocarbons in 1.0 nm square-shaped 1D channels of Co(BDP) show separation characteristics that are desirable from an industrial perspective. The channel dimension is large enough to allow the *p*-xylene molecules to align vertically. This leads to a good packing of the *para* isomer within the 1D channels. The simulations of the pure component isotherms clearly demonstrate a higher adsorption loading of *p*-xylene than any of the other C₈ hydrocarbons. Breakthrough simulations confirm that *p*-xylene is the last component to emerge from the fixed bed (Figure S31).

Jin et al.^[20] have presented isotherm data for xylene isomers in JUC-77 which is a MOF that has rhombus-shaped channels running in two perpendicular directions. The size of the channels is such as to favor only *p*-xylene that has the smallest width; this results in *para*-selectivity in separation. The simulations of pure component isotherms and breakthrough simulations (Figures S34 and S35) confirm the *para* selectivity observed in the experiments. Diffusional limitations are expected to be of paramount importance for JUC-77.

MAF-X8 possesses the right channel dimensions for the stacking of *para*-xylene to occur. MAF-X8 is a Zn^{II} pyrazolate-carboxylate framework whose synthesis has been reported by He et al.^[21] We observed a high adsorption selectivity of *p*-xylene with respect to *o*- and *m*-xylene and ethylbenzene; see mixture isotherm data in Figure 3a. The ideal adsorption solution theory (IAST) prediction of the mixture equilibrium based on the pure components is of excellent accuracy as verified by molecular simulations of mixture adsorption. The breakthrough simulations presented in Figure 3b confirm the strong *para* selectivity. The presence of benzene and toluene in the feed mixture does not seem to

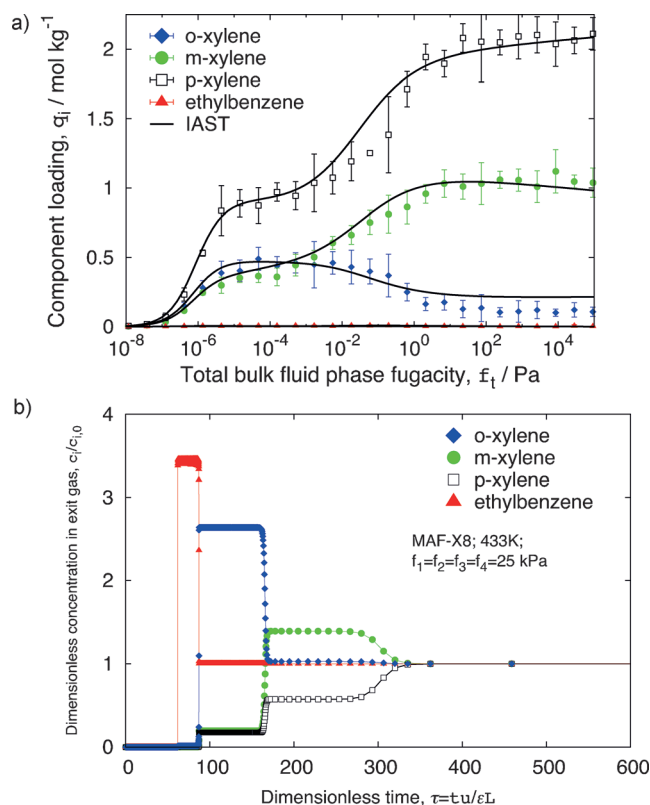


Figure 3. Xylene separation at 433 K using MAF-X8. a) Equimolar mixture isotherms and IAST prediction based on pure component isotherms. b) Simulated step breakthrough at 25 kPa partial pressure. The IAST prediction is in excellent agreement with the mixture simulations and its validation is important because IAST is the basis for the breakthrough computations. The mixture and breakthrough simulations show high *p*-xylene selectivity combined with a high *p*-xylene loading in the mixture (about 2.2 mol kg⁻¹ at 1 bar). At 433 K the bulk fluid is in the liquid phase if the total mixture fugacity is higher than about 1 MPa. Our breakthrough simulations operate at 100 kPa, and therefore are somewhat conservative with regard to separation.

influence the sharp separations that are achievable with MAF-X8 (Figure S43b). In contrast to CoBDP, MAF-X8 is commensurate with the structure in all three coordinate directions. Snapshots (Figure 4) highlight that the high selectivity is due to stacking. This raises the question: “How good is molecular stacking compared to other separation mechanisms?”

Figure 5 compares the separation characteristics of materials that are selective to *p*-xylene adsorption. We note that MAF-X8 has nearly the same adsorption selectivity as BaX, but has a significantly higher capacity to adsorb *p*-xylene. This higher capacity of MAF-X8 results in a significantly longer cycle time, which implies that less frequent regeneration will be required. All other MOFs appear to be significantly poorer in selectivity as compared to BaX and MAF-X8. The other MOFs are also lower in *p*-xylene adsorption capacity. This shows that molecular stacking is able to make (near) optimal use of the available pore volume.

Using state-of-the-art molecular simulation methodologies, we have systematically screened a wide variety of

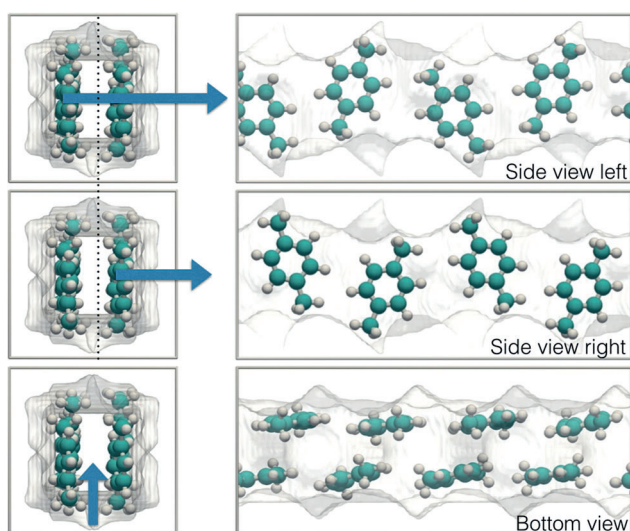


Figure 4. Stacking of *p*-xylene in the MAF-X8 structure. Note that *p*-xylene is commensurate in three directions: it fits perfectly length-wise, it forms two layers that fit snugly, and along the channel *p*-xylene stacks in an alternating fashion.

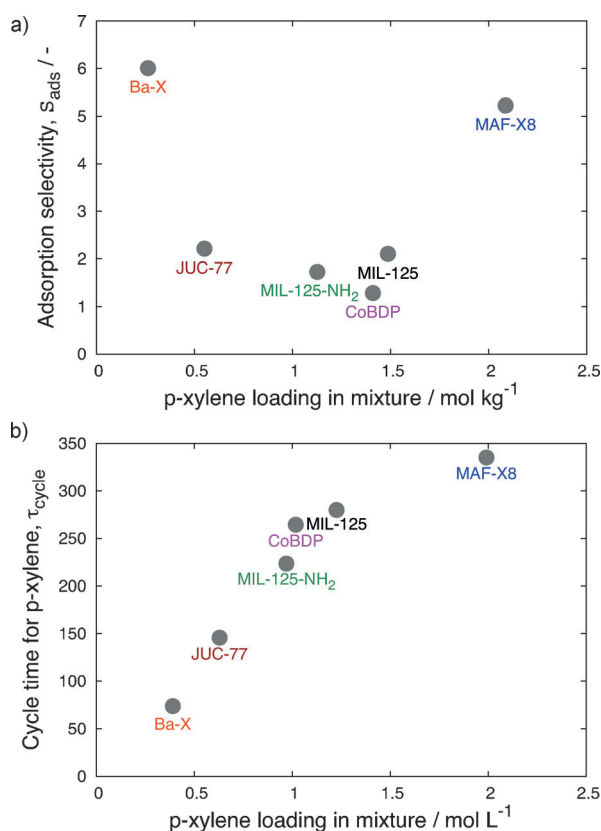


Figure 5. Comparison of *p*-xylene selective MOFs: a) Adsorption selectivity versus *p*-xylene capacity. b) Comparison of adsorption selectivity versus *p*-xylene cycle time for various MOFs. The adsorption selectivity is defined as $3q_3/(q_1+q_2+q_4)$ where 1 = *o*-xylene, 2 = *m*-xylene, 3 = *p*-xylene, and 4 = ethylbenzene. We define the cycle time for *p*-xylene as the dimensionless time, τ_{cycle} , at which the concentration of the gas at the outlet is 99 % of the value at the inlet.

zeolites and metal–organic frameworks (MOFs) to investigate the possibilities of achieving separation performances that are superior to BaX. Our investigations have highlighted the crucial importance of channel dimensions on separations. MOFs such as MIL-47(V), MIL-53(Al), MOF-CJ3, UiO-66, and Zn(bdc)dabco exhibit selectivity towards *o*-xylene, a feature that is not desirable in industrial practice. On the other hand, MAF-X8, Co(BDP), MIL-125(Ti), MIL-125(Ti)-NH₂, MFI, and JUC-77 have the desirable selectivity towards *p*-xylene isomers. Of these MOFs, MAF-X8 is particularly noteworthy because the channel dimensions and geometry allow efficient and commensurate stacking of *p*-xylene molecules. Such efficient stacking results in adsorption selectivities that are comparable to that of BaX. More importantly, the *p*-xylene adsorption capacity of MAF-X8 is significantly higher than that of BaX. Consequently, the cycle times for *p*-xylene are found to be about a factor of 4.5 longer with MAF-X8 and this is expected to result in significant process improvements.

Experimental Section

The adsorption computations are performed using the configurational-bias Monte Carlo (CBMC), continuous fractional component Monte Carlo (CFCMC),^[22] and configurational-bias continuous fractional component Monte Carlo (CB/CFCMC)^[23] algorithms in the grand-canonical ensemble. The systems are modeled in full atomistic detail (all atom model) using classical force fields:^[24] OPLS for the adsorbents, DREIDING for the MOFs, and TraPPE for the zeolites.

Using the dual-site Langmuir–Freundlich fits of the pure component isotherms, breakthrough calculations were carried out by solving a set of partial differential equations for each of the species in the gas mixture.^[25]

Received: March 3, 2014

Revised: April 9, 2014

Published online: June 10, 2014

Keywords: adsorption · stacking interactions · MOFs · selective separation · xylenes

- [1] E. W. Flick in *Industrial solvent handbook*, 5th ed., Noyes Data Corporation, Westwood, **1998**.
- [2] J. Scheirs, T. E. Long in *Industrial Modern Polyesters: chemistry and technology of polyesters and copolyesters*, Wiley, Chichester, **2003**.
- [3] J. Vicens, A. E. Armah, S. Fujii, K.-I. Tomita, *J. Inclusion Phenom. Macrocyclic Chem.* **1991**, 10, 159–163.
- [4] D. Peralta, K. Barthelet, J. Pérez-Pellitero, C. Chizallet, G. Chaplais, A. Simon-Masseron, G. D. Pirngruber, *J. Phys. Chem. C* **2012**, 116, 21844–21855; K. A. O. Santos, A. A. Dantas Neto, M. C. P. A. Moura, T. N. Castro Dantas, *Braz. J. Petroleum Gas* **2011**, 5, 255–268.
- [5] R. Q. Snurr, A. T. Bell, D. N. Theodorou, *J. Phys. Chem.* **1993**, 97, 13742–13752.
- [6] “Molecular simulation studies of gas adsorption and separation in metal–organic frameworks”: P. Z. Moghadam, PhD thesis, University of Edinburgh, **2012**.
- [7] M. Minceva, A. E. Rodrigues, *Chem. Eng. Res. Des.* **2004**, 82, 667–681.
- [8] M. Minceva, P. S. Gomes, V. Meshko, A. E. Rodrigues, *Chem. Eng. J.* **2008**, 140, 305–323.

- [9] R. Krishna, *Microporous Mesoporous Mater.* **2014**, *185*, 30–50.
- [10] J. M. Castillo, T. J. H. Vlugt, S. Calero, *J. Phys. Chem. C* **2009**, *113*, 20869–20874.
- [11] V. Finsy, H. Verelst, L. Alaerts, D. De Vos, P. A. Jacobs, G. V. Baron, J. F. M. Denayer, *J. Am. Chem. Soc.* **2008**, *130*, 7110–7118.
- [12] T. Remy, G. V. Baron, J. F. M. Denayer, *Langmuir* **2011**, *27*, 13064–13071.
- [13] L. Z. Fang, S. R. Zheng, J. B. Tan, S. L. Cai, J. Fan, X. Yan, W. G. Zhang, *J. Chromatogr. A* **2013**, *1285*, 132–138.
- [14] M. P. M. Nicolau, P. S. B rcia, J. M. Gallegos, J. A. C. Silva, A. E. Rodrigues, B. Chen, *J. Phys. Chem. C* **2009**, *113*, 13173–13179.
- [15] P. S. B rcia, D. Guimar es, P. A. P. Mendes, J. A. C. Silva, V. Guillermin, H. Chevreau, C. Serre, A. E. Rodrigues, *Microporous Mesoporous Mater.* **2011**, *139*, 67–73.
- [16] M. A. Moreira, J. C. Santos, A. F. P. Ferreira, J. Loureiro, F. Ragon, P. Horcajada, K. E. Shim, Y. K. Hwang, U. H. Lee, J. S. Chang, C. Serre, A. E. Rodrigues, *Langmuir* **2012**, *28*, 5715–5723.
- [17] F. Vermoortele, M. Maes, P. Z. Moghadam, M. J. Lennox, F. Ragon, M. Boulhout, S. Biswas, K. G. M. Laurier, I. Beurroies, R. Denoyel, M. Roeffaers, N. Stock, T. D ren, C. Serre, D. E. De Vos, *J. Am. Chem. Soc.* **2011**, *133*, 18526–18529.
- [18] M. A. Moreira, J. C. Santos, A. F. P. Ferreira, J. Loureiro, F. Ragon, P. Horcajada, P. G. Yot, C. Serre, A. E. Rodrigues, *Langmuir* **2012**, *28*, 3494–3502.
- [19] M. A. Moreira, J. C. Santos, A. F. P. Ferreira, J. Loureiro, F. Ragon, P. Horcajada, P. G. Yot, C. Serre, A. E. Rodrigues, *Microporous Mesoporous Mater.* **2012**, *158*, 229–234.
- [20] Z. Jin, H. Y. Zhao, X. J. Zhao, Q. R. Fang, J. R. Long, G. S. Zhu, *Chem. Commun.* **2010**, *46*, 8612–8614.
- [21] C. T. He, J. Y. Tian, S. Y. Liu, G. Ouyang, J. P. Zhang, M. Chen, *Chem. Sci.* **2013**, *4*, 351–356.
- [22] W. Shi, E. J. Maginn, *J. Chem. Theory Comput.* **2007**, *3*, 1451–1463.
- [23] A. Torres-Knoop, S. P. Balaji, T. Vlugt, D. Dubbeldam, *J. Chem. Theory Comput.* **2014**, *10*, 942–952.
- [24] W. L. Jorgensen, D. S. Maxwell, J. Tirado-Rives, *J. Am. Chem. Soc.* **1996**, *118*, 11225–11236; S. L. Mayo, B. D. Olafson, W. A. Goddard, *J. Phys. Chem.* **1990**, *94*, 8897–8909; P. Bai, M. Tsapatsis, J. I. Siepmann, *J. Phys. Chem. C* **2013**, *117*, 24375–24387.
- [25] R. Krishna, J. R. Long, *J. Phys. Chem. C* **2011**, *115*, 12941–12950.